Measurement of the ^{236}U(n, f) cross section for neutron energies from 0.4 MeV to 40 MeV from the back-streaming white neutron beam at the China Spallation Neutron Source

Zhizhou Ren,[1] Yiwei Yang,[1] Jie Wen,[1] Hairui Guo,[2] Zhongwei Wen,[1] Rong Liu,[1,*] Zijie Han,[1] Weili Sun,[2] Xingyan Liu,[1] Qiping Chen,[1] Tao Ye,[2] Qi An,[3,4] Huaiyong Bai,[5] Jie Bao,[6] Ping Cao,[3,4] Yonghao Chen,[7,8] Pinjing Cheng,[9] Zengqi Cui,[5] Ruirui Fan,[3,7,8] Changqing Feng,[3,4] Minhao Gu,[3,7] Fengqin Guo,[7,8] Changcai Han,[10] Guozhu He,[6] Yongcheng He,[7,8] Yuefeng He,[9] Hanxiong Huang,[6] Weiling Huang,[7,8] Xiru Huang,[3,4] Xiaolu Ji,[3,7] Xuyang Ji,[3,11] Haoyu Jiang,[5] Wei Jiang,[7,8] Hantao Jing,[7,8] Ling Kang,[7,8] Mingtao Kang,[7,8] Bo Li,[7,8] Lun Li,[7,8] Qiang Li,[7,8] Xiao Li,[7,8] Yang Li(a),[3,7] Yang Li(b),[7,8] Shubin Liu,[3,4] Guangyuan Luan,[6] Yinglin Ma,[7,8] Changjun Ning,[7,8] Binbin Qi,[3,4] Jie Ren,[6] Xichao Ruan,[6] Zhaohui Song,[10] Hong Sun,[7,8] Xiaoyang Sun,[7,8] Zhijia Sun,[3,7,8] Zhixin Tan,[7,8] Hongqing Tang,[6] Jingyu Tang,[7,8] Pengcheng Wang,[7,8] Qi Wang,[6] Taofeng Wang,[12] Yanfeng Wang,[7,8] Zhaohui Wang,[6] Zheng Wang,[7,8] Qingbiao Wu,[7,8] Xiaoguang Wu,[6] Xuan Wu,[7,8] Likun Xie,[3,11] Han Yi,[7,8] Li Yu,[7,8] Tao Yu,[3,4] Yongji Yu,[7,8] Guohui Zhang,[5] Jing Zhang,[7,8] Linhao Zhang,[7,8] Liying Zhang,[3,7,8] Qingmin Zhang,[13] Qiwei Zhang,[6] Xianpeng Zhang,[10] Yuliang Zhang,[7,8] Zhiyong Zhang,[3,4] Yingtan Zhao,[13] Liang Zhou,[7,8] Zuying Zhou,[6] Danyang Zhu,[3,4] Kejun Zhu,[3,7] and Peng Zhu[7,8]

[1]*Institute of Nuclear Physics and Chemistry, China Academy of Engineering Physics, Mianyang 621900, China*
[2]*Institute of Applied Physics and Computational Mathematics, Beijing 100088, China*
[3]*State Key Laboratory of Particle Detection and Electronics, China*
[4]*Department of Modern Physics, University of Science and Technology of China, Hefei 230026, China*
[5]*State Key Laboratory of Nuclear Physics and Technology, School of Physics, Peking University, Beijing 100871, China*
[6]*Key Laboratory of Nuclear Data, China Institute of Atomic Energy, Beijing 102413, China*
[7]*Institute of High Energy Physics, Chinese Academy of Sciences (CAS), Beijing 100049, China*
[8]*Spallation Neutron Source Science Center, Dongguan 523803, China*
[9]*University of South China, Hengyang 421001, China*
[10]*Northwest Institute of Nuclear Technology, Xi'an 710024, China*
[11]*Department of Engineering and Applied Physics, University of Science and Technology of China, Hefei 230026, China*
[12]*School of Physics, Beihang University, Beijing 100083, China*
[13]*Xi'an Jiaotong University, Xi'an 710049, China*

(Received 8 April 2020; revised 16 July 2020; accepted 29 July 2020; published 8 September 2020; corrected 8 January 2021)

A new measurement of the neutron-induced fission cross section of ^{236}U relative to the standard ^{235}U(n, f) cross section from 0.4–40 MeV was carried out by the time-of-flight method and a multicell fast fission ionization chamber at the China Spallation Neutron Source-Back-n white neutron source. The measured resonance peaks and the distribution of fission event-energy spectrum from the ^{235}U(n, f) reaction are in good agreement with that of the ENDF/B-VIII.0 evaluation, which confirms the reliability of the experimental setup. The measured ^{236}U /^{235}U fission cross section ratios in 0.4–40 MeV neutron energy region are compared to previous measurements. The ^{236}U fission cross section with the relative experimental uncertainty of 11.2%–2.9% in 0.4–1 MeV and 2.9%–2.8% in 1–40 MeV is determined and compared to calculation, previous measurements, and main evaluations. The present theoretical result with calculation program UNF reproduces the experimental data and the LANSCE data better than ENDF/B-VIII.0 evaluation does in the secondary fission region. The result confirms current evaluations from 0.4–40 MeV in most energy points and provides the experimental data for evaluating the discrepancies in the relevant energy region.

DOI: 10.1103/PhysRevC.102.034604

I. INTRODUCTION

The fission cross-section data is the most important nuclear reaction data for energy production, especially in the applications related to the future production of clean, sustainable, and safe nuclear energy as well as for nuclear waste transmutation [1]. Therefore, the accurate measurement of the neutron-induced fission cross section is of great significance for the design of advanced nuclear reactors and other nuclear systems. The ^{236}U nuclide in the Th/U fuel cycle plays a similar role as the ^{242}Pu nuclide in the U/Pu fuel cycle, and is of interest because of its buildup in the equilibrium fuel composition. The ^{236}U fission cross section with 5% accuracy is required in some nuclear systems based on the Th/U cycle [2].

With the development of the method of measuring fission cross section, the mainstream method by time-of-flight (TOF) and white neutron source is used to measure fission cross

*Corresponding author: liurongzy@163.com

section in a wide energy region. Parker *et al.* [3] has measured neutron-induced fission cross sections of ^{236}U with a white neutron source using a parallel-plate ionization chamber at the LANCSE facility with a 56 m flight distance. In this experiment, four new neutron-induced fission resonances of ^{236}U were observed in 1–12 keV energy region. Behrens and Carlson [4] has measured the neutron-induced fission cross sections of ^{236}U relative to ^{235}U from 0.1–30 MeV at Lawrence Livermore National Laboratory by using time of flight with 15.7 m flight path and the total uncertainty is from 6.5%–4.4% in 0.3–30 MeV. Lisowski *et al.* [5] measured ^{236}U /^{235}U fission cross-section ratios from 0.5–400 MeV at the LANSCE Linac and WNR facility and the information of uncertainty is not given explicitly.

Recently, a latter measurement was carried out at n-TOF facility at CERN from 170 meV to 2 MeV with a multistack fast ionization chamber. The flight path is 186.4 m and the protons bunches width is 7 ns, which leads to a good accuracy up to 2 MeV and a statistical error from 10.5%–0.75% in 0.5–2 MeV [6]. Hughes *et al.* [7] carried out the surrogate ratio method measurements for (p, d) (p,d) and (p,t) reactions on uranium nuclei. ^{236}U and ^{238}U targets were bombarded with 28 MeV protons and the light ion recoils and fission fragments were detected using the Silicon Telescope Array for Reaction Studies detector array at the 88 Inch Cyclotron at Lawrence Berkeley National Laboratory. The resulting ^{236}U /^{235}U fission cross-section ratios show relatively good agreement with accepted values up to 5 MeV. Tovesson *et al.* [8] measured fast neutron-induced fission cross sections of ^{236}U in a wide region from 200 keV to 200 MeV at LANCSE by using parallel-plate ionization chambers within a uncertainty up to 13.2%.

Current evaluated nuclear data in libraries are mainly based on these measurements. Few data have been measured resulting in discrepancies in the latest evaluations. In some points, these measurements do not agree well with each other and the discrepancies are over than 7% [9]. Hence, a new measurement is essential for providing experimental data to improve the evaluations.

In this work, the new measurement of ^{236}U fission cross sections relative to ^{235}U from 0.4–40 MeV has been carried out at the China Spallation Neutron Source (CSNS)-Back-n white neutron source (WNS) [10,11] with Fast Ionization Chamber Spectrometer for Fission Cross Section Measurement (FIXM) based on a multicell fast fission ionization chamber (FIC) and high-purity uranium isotope samples [12]. The experiment method is introduced in Sec. II. After a brief description of the white neutron source, FIC chamber, and samples in Sec. III, data analysis is presented in Sec. IV. Results and discussion are in Sec. V. The conclusion is given in Sec. VI.

II. EXPERIMENTAL METHOD

The ^{236}U(n, f) cross section was measured by using the TOF method and CSNS white neutron source with a multicell fast fission ionization chamber, which is relative to the standard ^{235}U(n, f) cross section. The ^{235}U(n, f) cross section is a standard at 0.0253 eV and from 0.15–200 MeV. Uncertainties in the standard file are $<1\%$ in the neutron energy range between 150 keV and 300 keV, 0.5%–1.0% between 300 keV and 20 MeV, and increase from1.0%–4.5% between 20 MeV and 200 MeV [8]. The ^{236}U /^{235}U neutron-induced fission cross section ratio can be determined from the background-subtracted fission events $C(En)$ according to the Eq. (1).

$$\frac{\sigma_6(E_n)}{\sigma_5(E_n)} = \frac{C_6(E_n)}{C_5(E_n)} \times \frac{N_5}{N_6} \times \frac{\varepsilon_5}{\varepsilon_6} \times P \tag{1}$$

The subscripts 6 and 5 refer to the ^{236}U and ^{235}U, N is the number of fission atoms in the sample used in the measurements, ε is the detection efficiency for fission events. P represents the correction for the measurement. The measurements are performed relative to a ^{235}U(n, f) sample in the chamber.

III. EXPERIMENTAL SETUP

A. CSNS Back-n white neutron source

CSNS is a large scientific facility completed in early 2018, which is mainly for multidisciplinary research on material characterization using neutron scattering techniques [10,13]. Back-streaming neutrons through the incoming proton channel at the spallation target station have been exploited as a white neutron beam line for nuclear data measurements.

The 1.6 GeV protons with a 25 Hz repetition is produced by CSNS to impinge onto a thick tungsten target to provide white neutron beam (the back-streaming neutrons). Proton bunches power will be increased from 10–100 kW in the first phase of CSNS. With the thick tungsten target and the water serving as coolant through it, the neutron beam at 80 m from the target is in the order of 5.76×10^6 n/cm^2/s at 100 kW, which has an excellent energy spectrum spanning from 1 eV to 100 MeV [11].

The measurements were performed in the dedicated single-bunch mode and the beam power is about 10 kW. The size of neutron beam spot is Φ 60 mm. In this mode, the proton bunches are accumulated in the Rapid Cycling Synchrotron (RCS) and each Gauss-type bunch has a length of about 41 ns (FWHM) [14].

B. Detector and data acquisition

The multicell fast fission ionization chamber [12] has been designed for the fission cross-section measurement, which was mounted at the end station 2 at the CSNS-WNS. The ϕ 300 mm $\times$ 300 mm cylindrical shell of the ionization chamber was made of stainless steel 5 mm thick and the ϕ 80 mm

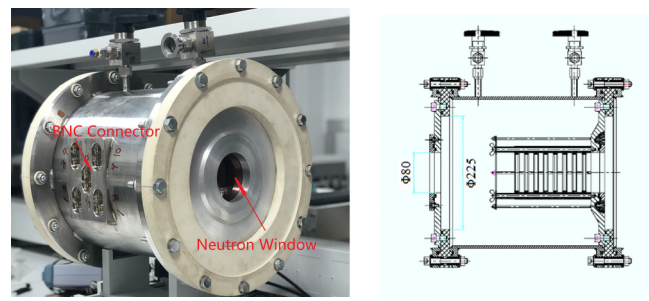

FIG. 1. Photo (left) and schematic diagram (right) of the FIC used in the measurement.

TABLE I. Characteristics of the samples used in the measurement.

Sample	Mass (mg)	Uncertainty (%)	Diameter (cm)	Mass Thickness (mg/cm^2)	Uncertainty (%)
^{235}U-1	5.1729	0.98	4.974	0.266	1.02
^{235}U-2	5.7067	1.01	4.976	0.293	1.05
^{236}U-1	2.2103	0.98	4.969	0.114	1.02

window sealed with a Kapton film 100 μm thick is located in the center of one of the chamber caps. The chamber is filled with a gas mixture of 90% Ar and 10% CH_4 at a pressure of 800 mbar. A stack of fission cells was mounted along the direction of the neutron beam inside the chamber. The detail structure of the FIC is shown in Fig. 1.

Each cell consists of two Φ 80 mm electrodes. The aluminum anode collects ionization signals by connection to a preamplifier while the stainless-steel cathode plated with the fission material is connected to the ground. The 5-mm-wide gap and a high voltage (+200V) between electrodes was designed in order to provides electrons enough drift velocity, about 6×10^4 m/s.

The eight-channel preamplifier MSI-8 has been chosen for the detector because of its large amplification, which could record the α-particle signal from the radioactive decay or from the competing (n, α) reactions in the lower limit of the data acquirement (DAQ) system (50–100 mV). The DAQ system used to digitize and store signals mainly includes a signal conditioning module (SCM) for the timing output of MSI-8, a field digitizing module (FDM) with 12-bit resolution and 1 G samples/s digitization rate, a trigger and clock module (TCM) and a data center for storing waveform data. The memory time of FDM is up to 30 ms to store fission events down to the thermal energy region [12].

C. Samples

Three uranium isotope samples are used in this measurement:^{235}U-1, ^{235}U-2, and ^{236}U-1. The uranium fission materials were electroplated on the backings of stainless steel in the form of U_3O_8. The diameter of the deposit is about 50 mm, which was exactly measured by the α-particle imaging method. The masses of the deposits were determined by the α-particle spectra measured with a PIPS semiconductor detector in a small solid angle device. The number of uranium atoms in the deposit was calculated by the decay rates and α-particle intensities. The results of quantified mass, mass thickness, and uncertainty are listed in Table I.

TABLE II. The compositions of high-purity uranium samples.

Sample	Isotopes	Abundance (%)	Relative Uncertainty (%)
^{235}U	^{234}U	1.2560×10^{-3}	1.3×10^{-1}
	^{235}U	$9.9985\times10^{+1}$	6.8×10^{-6}
	^{236}U	4.1160×10^{-3}	1.2×10^{-1}
	^{238}U	9.6260×10^{-3}	3.9×10^{-2}
^{236}U	^{234}U	2.7660×10^{-5}	$4.0\times10^{+0}$
	^{235}U	6.3447×10^{-3}	6.5×10^{-2}
	^{236}U	$9.9944\times10^{+1}$	5.7×10^{-5}
	^{238}U	4.9554×10^{-2}	1.2×10^{-1}

The ^{236}U sample was enriched to 99.944% and the ^{235}U sample was enriched to 99.985%. The compositions of high-purity uranium samples are shown in Table II. The impurities of samples measured by using a mass spectrometry have good agreements with the α-particle spectra, which confirmed the accuracy of the impurity measurement. The mass uncertainty of each sample is given by the quantitative experiment, which is obtained by calculating each influence factor with error transfer formula. The uncertainty of mass thickness was calculated by coupling the mass uncertainty with the diameter uncertainty.

The image of the ^{236}U deposit was obtained by an α-sensitive imaging plate and the fluorescence intensity distribution reflects the density distribution of uranium atoms. The ^{236}U sample photo and its mass distribution image in which the pixel size is 0.2 mm × 0.2 mm are shown in Fig. 2. α counting over the surface of the samples was used to determine the uniformity of the deposits. Referred to the resolution of the section of white neutron beam on the front surface of the samples (Sec. III C), the nonuniformity of the deposit is about 21% at a resolution of 2 mm × 2 mm.

IV. DATA ANALYSIS

The FIC was aligned to the center of the neutron beam by laser collimation at the end station 2. Because of a Cd foil 1 mm thick located at the neutron beam window, the thermal neutrons were absorbed and will not be recorded. The DAQ acquisition time window was set to 10 ms, which is corresponding to an energy about 0.3 eV of neutrons in about 76 m flight path. The raw event data are analyzed by means of C++ program based on the ROOT software package developed by CERN [15]. The pulse height of each signal

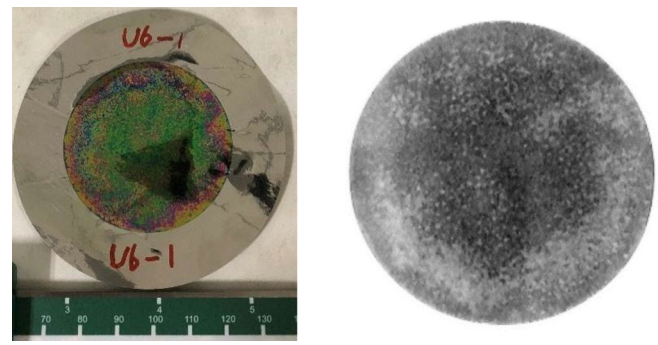

FIG. 2. The ^{236}U sample photo (left) and its mass distribution image (right). Nuclides are more in the middle and less around.

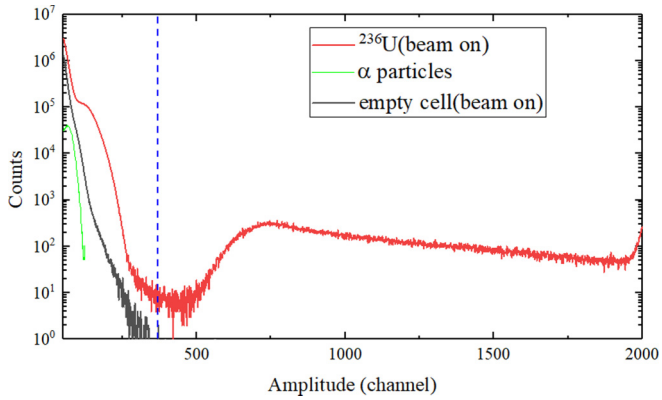

FIG. 3. The amplitude spectra of the ^{236}U cell measured with neutron beam (red line), the residual α particles measured without neutron beam and normalized by the number of corresponding proton bunches (green line) and the background measured by using empty cell with neutron beam (black line).

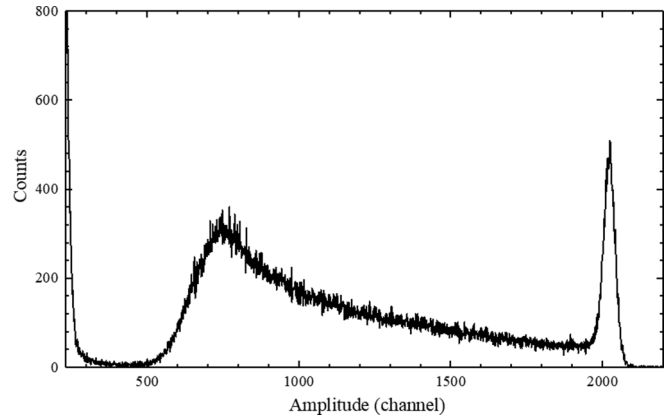

FIG. 4. The amplitude spectrum of ^{236}U cell.

was returned by routines to obtain amplitude spectrum and the time information was used to calibrate the flight time of each neutron in order to determine the neutron energy. Further analysis is performed to correct for background events, beam nonuniformity, and sample mass.

A. Amplitude spectrum and detection efficiency

The amplitude spectrum of ^{236}U cell is used to distinguish fission events from α particle, γ flash, and electronic noise. The γ flash of 1–2 MeV was produced by the target nucleus deexcitation. The detector response for (n, α) events from the sample backing was measured by a blank backing and the decay radiation was measured without neutron beam. The amplitude spectra of the ^{236}U cell and empty cell measured with neutron beam and without neutron beam are shown in Fig. 3.

The main sources of background detected by FIC are the contribution of α particles from the ^{236}U decay and the signal collected by empty cell for recording effects of neutron reacting with backing and aluminum collector. The blue line is the threshold of ^{236}U cell. The α signals, γ flash, and electronic noise distribute in low amplitude region while the amplitude of fission fragments is continuous and widely distributed. The background signal found below threshold and few counts above threshold was to be neglected.

After the ^{236}U(n, f) amplitude spectrum is subtracted the residual α particles and the background, the detector response could separate fission events from background clearly, as shown in Fig. 4. The black line indicates the data subtracted the residual α particles and the background. An obvious valley was observed below 500 channels and the threshold was set at channel 375 to analyze detection efficiency. There is a peak around 2000 ch in the spectrum, which is caused by a signal saturation effect of the SCM.

There is a count valley from about 250 channels to 500 channels and the peak-to-valley ratio is about 38:1. The pulse-height threshold (375 channels) was selected in middle of the smoother area in the count valley. The fission events were selected by applying a pulse-height threshold and subtracting the measured background.

The loss of fission events mainly comes from the pulse-height threshold setting in amplitude spectrum and self-absorption. The efficiency ε for recording fission fragments can be calculated via Eq. (2) [14]. The N_U is the total count of fission events above the threshold and the N_L stands for the lost count of fission events below the threshold. N_L calculated by the assumption that there are a constant number of fission events per pulse-height bin below threshold (flat tail assumption). R is the average range of fission fragments in uranium deposit, and its value is 7.5 ± 0.5 mg/cm^2 . t is the mass thickness of deposit. The efficiencies of the two ^{235}U cells and ^{236}U cell are 93.7%, 93.7%, and 97.8%, respectively. A large thickness of ^{235}U sample shown in Table I result in more self-absorption and lower the efficiency. The uncertainty of the efficiencies is about 0.47%, 0.45%, and 0.26%, which is mainly derived from the statistical uncertainty of fission events counting above and below the threshold

$$\varepsilon = \left(1 - \frac{\mathrm{t}}{2R}\right) \times \left(1 - \frac{N_L}{N_U}\right) \tag{2}$$

B. Neutron-energy calibration

The TOF of neutron (TOF_n) was calculated by Eq. (3) [12], where T_f is the production time of the fission relative to the zero time point T_0, which is the time of tungsten target bombarded by proton bunches; T_n the production time of the neutron that caused the fission event relative to T_0; T_γ is the time of its corresponding γ flash recorded by the detector; TOF_γ is the flight time of the γ flash from the target to the detector. The T_{PULSE} is the difference in the production time between this neutron and γ flash. In fact, T_{PULSE} can not be accurately known because of the 41 ns proton pulse width. We take T_{PULSE} as 0, and its uncertainty is 41 ns. The TOF_γ could be calculated via flight distance with high accuracy and the T_f could also be well determined because of the good SNR (signal-to-noise ratio).

$$\begin{aligned} TOF_n &= T_f - T_n = T_f - (T_\gamma - TOF_\gamma + T_{\mathrm{pulse}}) \\ &= T_f - T_\gamma + TOF_\gamma. \end{aligned} \tag{3}$$

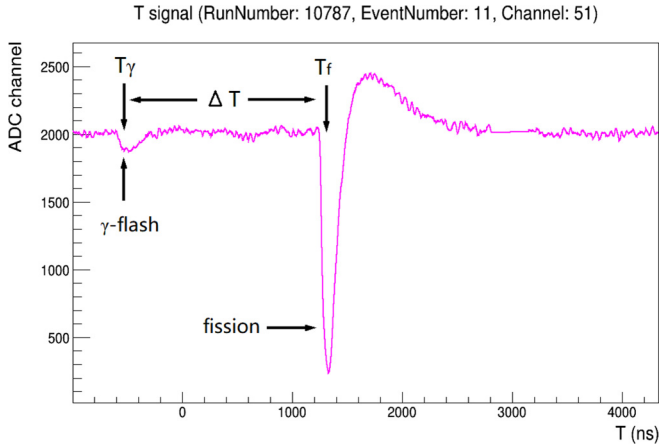

FIG. 5. The waveform of the γ flash and fission measured by ^{236}U cell.

As some big random noises were added to the original constant signals, the actual signals of γ flash acquired by the DAQ system were cluttered and totally different. Therefore, the random noises would cancel each other when signals of γ flash were superimposed, while the original constant signal would be retained. According to this principle, to reduce the influence of the random noises, multiple γ-flash signals (over 10000) were averaged to create a standard γ-flash signal to determine the start time of all the γ-flash signals. The result of the $T\gamma$ calibration for two ^{235}U cells and one ^{236}U cell are –574.8 ns, –573.9 ns, and –574.5 ns, respectively. The typical waveform of γ flash and fission produced by the ^{236}U cell is shown in Fig. 5. The rise and fall time of ^{236}U fission signal are about 60 ns and 250 ns (from 10% to 90%), respectively.

The flight distance was calibrated by the time difference of the neutron and the corresponding γ flash recorded by the DAQ system. The resonance peaks in the ^{235}U(n, f) cross section curve in 1–20 eV were selected to calculate the flight

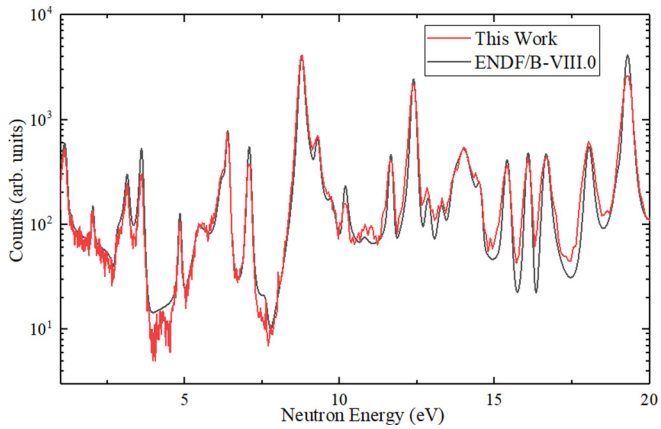

FIG. 6. Comparison of the energy spectrum measured by a ^{235}U cell (red line) with the ^{235}U(n, f) cross sections of ENDF/BVIII.0 (black line) normalized by the 8.774 eV ^{235}U(n, f) resonance peak. The two curves have a good agreement in trend, which is used for resonance peaks fitting and it confirms the reliability of the experiment and the method of data analysis.

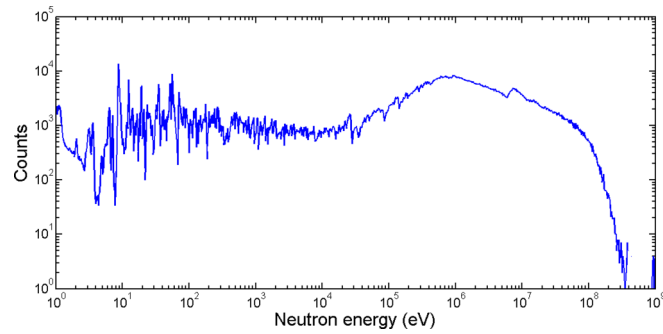

FIG. 7. The energy spectrum of the ^{235}U cell.

path distance L due to the high cross sections. The measured count rate as a function of neutron energy by the ^{235}U -1 cell and the evaluated cross sections of ENDF/B-VIII.0 [26] in 1–20 eV are shown in Fig. 6. To observe the resonance peaks more clearly, the energy spectrum is presented with 500 bins per decade (bpd). According to the energy points, the data from ENDF/B-VIII.0 are selected. The ENDF line in Fig. 6 did not fold with the time resolution of the measurement. Through the comparison and peak fitting, there is the good agreement in this energy range. The 8.77 eV peak is used to calibrate neutron flight path distance. The distance of this ^{235}U -1 cell to target is 75959 mm and the distances of other cells could be calculated by the physical distances between the cells.

The fission events-neutron energy spectra of ^{235}U and ^{236}U cells are shown in the Fig. 7 and Fig. 8, in which the preliminary results were used to see if the results are correct by analyzing the shape of spectra. The energy spectra have been divided by 100 bpd. The resonance peaks in the ^{235}U(n, f) cross section could be clearly observed in 1 eV to 1 keV neutron energy region. The distribution of the secondary chance fission [the $(n, n'f)$ reaction channel] could also be distinguished obviously in ^{235}U and ^{236}U neutron energy spectra in 6–8 MeV. In the ^{236}U neutron energy spectrum, the fission threshold energy above 0.69 MeV results in fewer counts below the threshold. These features proved the reliability of the measurement.

C. Sample and beam nonuniformity

The fission nuclides plated in backings and the section of white neutron beam on the front surface of the samples

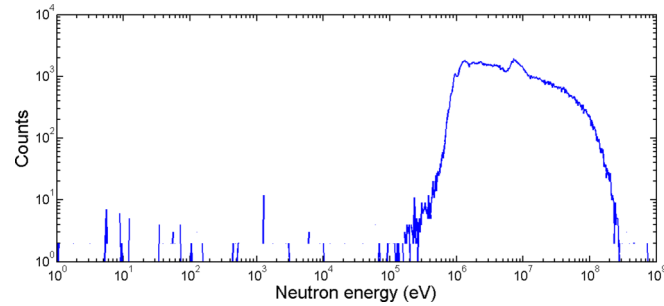

FIG. 8. The energy spectrum of the ^{236}U cell.

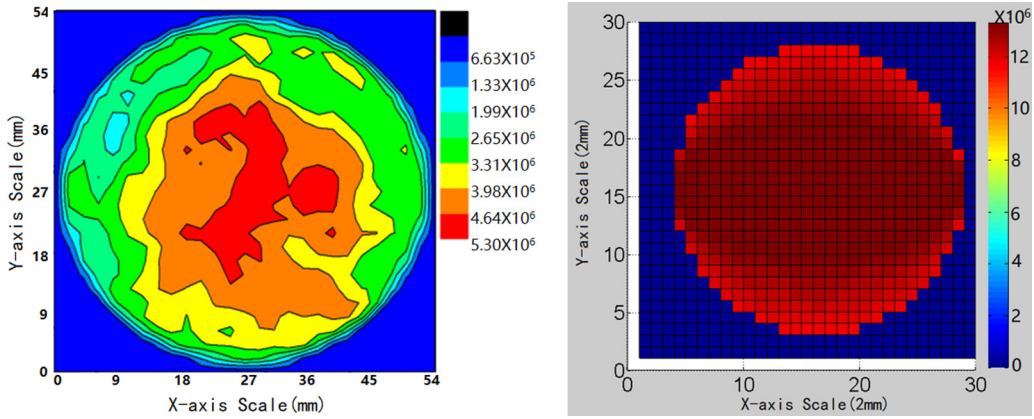

FIG. 9. The 2D image of the ^{236}U sample (left) and the white neutron beam (right).

are both not uniform, which have to be corrected in this experiment. The two-dimensional (2D) images of ^{236}U sample determined by the α-particle imaging method and the section of white neutron beam by calculation with the pixel size of 2 mm x 2 mm are shown Fig. 9. The nonuniformity of ^{236}U sample and the neutron beam section are about 21% and 10%, respectively.

The darker color at pixel represents more nuclides in the ^{236}U sample image and the higher intensity of the beam in the white neutron section. A variable Q is defined to correct the nonuniformity of samples and white neutron beam by multiplying the intensity of each pixel and the area of the pixel, then adding them up and comparing the value to the average. In order to eliminate the influence of anisotropy, Q is calculated from several angles and the Q difference from these angles is less than 0.15%. The average Q values of the ^{235}U and ^{236}U samples are 1.0043, 1.0030, and 1.0057 and the uncertainties are 0.12%, 0.09%, and 0.15%, respectively.

D. Neutron flux attenuation

In fact, as neutrons pass through the layers of the FIC, their fluxes gradually attenuate due to their interaction with stainless steel backings and aluminum collectors. The neutron flux attenuations in the FIC have been calculated and corrected by simulation. The simulation results show that the flux attenuation decreases with the increase of neutron energy. The neutron flux attenuations of the ^{235}U and ^{236}U samples are 0.02%–0.5% and 0.8%–1.6% at 0.4–40 MeV with the uncertainty less than 0.1% [14], respectively.

E. Dead time

This measurement was carried out with a single bunch mode and a 25 Hz repetition frequency in 10 kW beam power. Each sample set in the FIC was connected to the data acquisition system via an independent channel. The dead time of the system is mainly determined by the signal acquisition rate of the DAQ system and signal count rate in this experiment. The 1 G samples/s sampling rate of FDM is fully satisfied while the counting rate is about 10^3/s. Besides, the frame overlap also leads dead time. In this experiment, the ^{235}U counting rate is about 14 cps while ^{236}U is 2 cps. The probability of the frame overlap is less than 10^{-5} in each independent channel, which is estimated by counting rate and the FIXM resolution to waveform (60 ns). As a result, the dead time in this measurement is negligible.

F. Sample contamination

The correction for the impurity of the ^{236}U sample was also considered. The correction factor η can be calculated via Eq. (4), where δ is the abundance of related isotope and σ is the fission cross section. The ^{236}U sample was enriched to 99.944% with ^{235}U abundance less than 0.1% (Sec. III C). The ^{235}U nuclei mainly lead to a big background in 1eV to 0.1MeV energy range due to its larger fission cross section than that of ^{236}U. However, in 0.4–40 MeV, the uncertainty derived from the impurity of the ^{236}U sample is <0.02% and the ^{235}U sample is <0.01%.

$$\eta(E_n) = \frac{\delta_6 \cdot \sigma_6}{\delta_4 \cdot \sigma_4 + \delta_5 \cdot \sigma_5 + \delta_6 \cdot \sigma_6 + \delta_8 \cdot \sigma_8}. \quad (4)$$

V. RESULTS AND DISCUSSION

A. Measured ^{236}U /^{235}U fission cross-section ratio

According to the Eq. (1), the measured ^{236}U /^{235}U fission cross-section ratios are obtained from 0.4 MeV–40 MeV, in which the measured ^{235}U fission counts are derived from the addition of the two ^{235}U cell counts normalized by nucleus number. The experimental data is partitioned according to the logarithm of the neutron energy. In the range of 0.4–0.6 MeV, 0.6–9.5 MeV, and 9.5–40 MeV, the experiment data have been dived by 10 bpd, 50 bpd, and 25 bpd, respectively, which makes the data points more consistent with the energy resolution and reduces the statistical uncertainties in 0.4–0.6 MeV energy region. The results are shown in Fig. 10 and Fig. 11 and compared to previous measurements. In Fig. 11, the unlabeled uncertainties in the range of 0.4–0.7 MeV varies between 11%–6%. The different data sets are in good agreement. The current measurement agrees with the results by Tovesson *et al.* [8] and Sarmento *et al.* [6] better than Shpak *et al.* [16] over the 0.4–1 MeV energy range. In addition, as

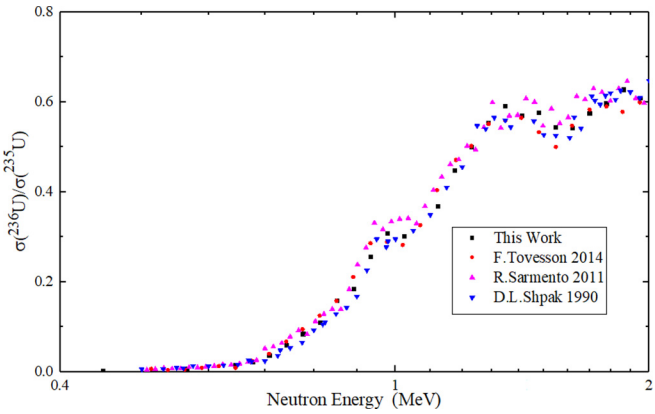

FIG. 10. Measured ^{236}U /^{235}U fission cross-section ratios compared to previous work from 0.4–2 MeV [6,8,16].

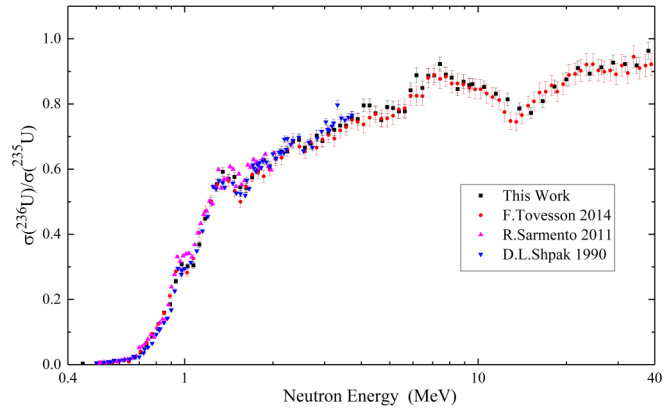

FIG. 11. Measured ^{236}U /^{235}U fission cross section ratios compared to previous work from 0.4–40 MeV [6,8,16].

shown in Fig. 11, the result measured in this experiment is in good agreement with that of Tovesson *et al.* in the 1–40 MeV energy range.

The uncertainty of measured ^{236}U /^{235}U fission cross section ratios mainly comes from the statistical error of fission events and the quantification of target nuclei. In the vicinity of the threshold, a sharp decrease of the statistical count rate of ^{236}U leads to a large uncertainty. The main contributions for experimental uncertainty were listed in Table III and the total experimental uncertainty is 11.2%–2.7% in 0.4–1 MeV and 2.7%–2.6% in 1–40 MeV, respectively. The statistical uncertainty of ^{235}U cell was derived from adding counts in the same bin measured by the two ^{235}U cells.

The total time resolution mainly comes from the pulse width of the proton beam, which is currently 41 ns (FWHM) and the time resolution of the detector system (5.7 ns). The relative energy resolution of a TOF facility taking into account the relativistic effect can be calculated by Eq. (5) and Eq. (6).

$$\frac{\Delta E}{E} = \gamma(\gamma+1)\sqrt{\left(\frac{\Delta T}{T}\right)^2 + \left(\frac{\Delta L}{L}\right)^2} \tag{5}$$

$$\gamma = \frac{1}{\sqrt{1-\left(\frac{v}{c}\right)^2}}. \tag{6}$$

T and L are the TOF and the flight path, respectively. $\Delta T/T$ and $\Delta L/L$ are their relative uncertainties. ΔT is the total time resolution, which is currently 41.4 ns. ΔL is caused by the moderation of the tungsten target and the surrounding coolant. The distribution of the moderation distance versus neutron energy simulated by FLUKA [17]. The representative energy resolution of this measurement was shown in Table IV.

B. ^{236}U(n, f) cross section

The measured ^{236}U(n, f) cross section could be calculated by introducing the standard ^{235}U(n, f) cross section in 0.4–40 MeV via Eq. (7) on the basis of Eq. (1), where $\sigma_5^{\rm eval}(En)$ is the evaluated fission cross section of ^{235}U from ENDF/B-VIII.0. The experimental uncertainty is 11.2%–2.9% in 0.4–1 MeV and 2.9%–2.8% in 1–40 MeV, respectively.

$$\sigma_6(E_n) = \frac{C_6(E_n)}{C_5(E_n)} \times \frac{N_5}{N_6} \times \frac{\varepsilon_5}{\varepsilon_6} \times P \times \sigma_5^{\rm eval}(E_n). \tag{7}$$

In the theoretical calculation, the fission reaction is regarded as a decay channel of equilibrium states. The unified Hauser-Feshbach and exciton model [18] is used to calculate the preequilibrium and equilibrium reaction processes. The neutron global optical potential from Ref. [19] is applied to calculate total and elastic scattering cross sections. The distorted wave Born approximation theory is used to give the direct inelastic scattering cross sections. The transmission coefficients and inverse cross sections of compound-process particle emission are calculated by the proton [19], deuteron [20], triton [21], and α [22] global optical potentials and γ strength function. The transmission coefficients at fission

TABLE III. The relative experimental uncertainty.

Content	^{235}U cell (%)	^{236}U cell (%)
C(En)	0.3–0.8	2.2–11.1 (0.4–1.0 MeV) 2.2–0.8 (1.0–40 MeV)
N	1.00	0.98
ε	0.47	0.26
Q	0.09	0.15
η	0.01	0.02
Total (^{236}U /^{235}U)	11.2–2.7 (0.4–1.0 MeV) 2.7–2.6 (1.0–40 MeV)	

TABLE IV. Representative energy resolution of this measurement.

En (MeV)	ΔT (ns)	ΔL(cm)	$\Delta E/E$
0.57	41.4	9.5	1.0×10^{-2}
1.02	41.4	15.3	1.5×10^{-2}
5.13	41.4	4.3	3.4×10^{-2}
9.34	41.4	4.9	4.6×10^{-2}
20.0	41.4	4.8	6.8×10^{-2}
38.1	41.4	6.4	9.6×10^{-2}

barriers are obtained by the Hill-Wheeler theory [23]. The continuum excited states are described by Gilbert-Comeron level density formula [24].

The present experimental data and calculated results compared with previous ones are given in Fig. 12 and Fig. 13. The solid squares and circles denote the present measured data and the data [8] measured at LANSCE in 2014, respectively. The triangles denote the data [7] measured by Hughes *et al.* via the surrogate-ratio method in 2012. The black, red, blue, and brown lines denote the present calculated, ENDF/B-VIII.0, JENDL-4.0, and CENDL-3.1 evaluations, respectively. The present theoretical result and experimental data are in good agreement, and consistent with the Tovesson data [8]. The average discrepancy of the experimental data and present theoretical result is about 3.0% in 1–20 MeV. The present theoretical result reproduces the two new sets of experimental data better than ENDF/B-VIII.0 evaluation does in the secondary fission region.

The comparison of the measured ^{236}U /^{235}U fission cross-section ratios and the ENDF/B-VIII.0 evaluation in 0.4–30 MeV is shown in Fig. 14. There are large discrepancies in 0.4–1.0 MeV, which is mainly caused by the large statistical uncertainty, especially below ^{236}U fission threshold energy (0.69 MeV). A better time resolution and more fission events are needed to precisely measure the cross section in this

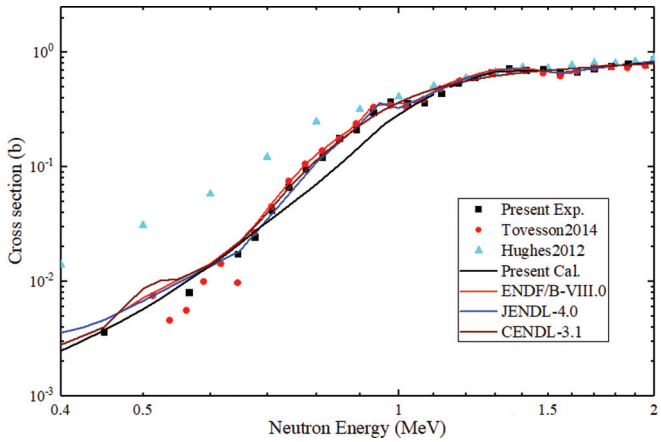

FIG. 12. Measured ^{236}U fission cross section compared to the calculation, previous data, the ENDF/B-VIII.0 and JENDL-4.0 evaluation from 0.4–2 MeV. The red, black, and cyan solid points denote the data measured in this experiment and that of Tovesson and Hughes. The black, red, blue, and brown lines denote the present calculated, ENDF/B-VIII.0, JENDL-4.0, and CENDL-3.1 evaluations, respectively [7,8,17,25–27].

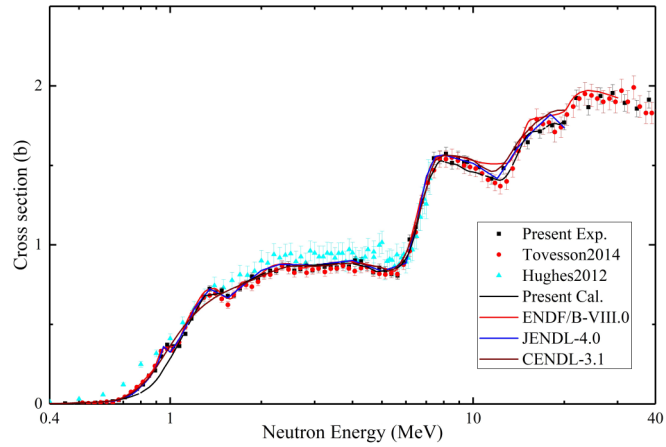

FIG. 13. Measured ^{236}U fission cross section compared to the calculation, previous data, the ENDF/B-VIII.0, JENDL-4.0 and CENDL-3.1 evaluations from 0.4–40 MeV [7,8,17,25–27].

region. The discrepancies are generally less than 5% in 1–30 MeV and the average discrepancies of the data is 2.8% in 1–30 MeV energy region.

VI. CONCLUSION

A new measurement of the ^{236}U /^{235}U fission cross section ratio from 0.4–40 MeV was carried out by the time-of-flight method and the multicell fast fission ionization chamber with the high-purity uranium isotope samples at CSNS-WNS. The measured resonance peaks and energy spectrum from the ^{235}U(n, f) reaction are in good agreement with that of the ENDF/B-VIII.0 evaluation, which was used to calibrate the flight distance and confirms the reliability of the experimental setup. The flight time of neutron was calculated through γ flash and the constant fraction timing method. The effect of neutron reacting with the stainless-steel backing and the aluminum collector was measured by using empty cell. The influences of the nonuniformity of white neutron beam, the attenuation of neutron flux in the detector, and the impurity isotope in the samples were all considered and the relevant corrections were made.

The ^{236}U /^{235}U fission cross-section ratios in 0.4–40 MeV neutron energy region with the experimental uncertainty of

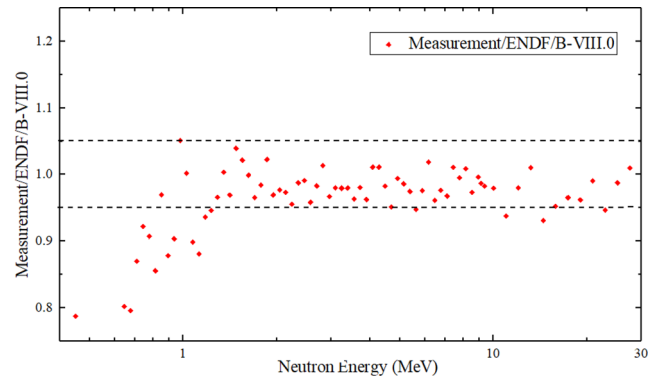

FIG. 14. The comparison of the measured ^{236}U /^{235}U fission cross section ratios and the ENDF/B-VIII.0 evaluation [25].

11.2%–2.7% in 0.4–1 MeV and 2.7%–2.6% in 1–40 MeV are obtained. The measured results generally agree with that from the ENDF/B-VIII.0 evaluation within the range of the uncertainty. Based on the standard ^{235}U fission cross section, the measured ^{236}U fission cross section with the experimental uncertainty of 11.2%–2.9% in 0.4–1 MeV and 2.9%–2.8% in 1–40 MeV is determined. The ^{236}U(n, f) cross section is analyzed by using the nuclear reaction theoretical model and calculation program UNF. The present theoretical result and experimental data are in good agreement, and consistent with the LANSCE data. The present theoretical result reproduces the two new sets of experimental data better than ENDF/B-VIII.0 evaluation does in some energy points. The result confirms current evaluations from 0.4–40 MeV in most energy points and provides experiment data for the discrepancies in the second and third fission energy region. The result proves that the multicell fast fission ionization chamber as well as the supporting electronic system has good performance and the method of data analysis is reliable. This experiment lays a good foundation for the further measurement of fission cross sections of other nuclides.

ACKNOWLEDGMENTS

This work is supported by the National Key Research and Development Plan (2016YFA0401603), the National Natural Science Foundation of China (11675155, 11790321), and Foundation of President of China Academy of Engineering Physics (YZJJLX2016003). The authors thank the CSNS Back-n Collaboration for their great work in neutron source operation and data acquisition.

[1] J. Y. Tang *et al.*, Key nuclear data measurements for advanced fission energy and white neutron source at CSNS, At. Energy Sci. Technol. **7**, 47 (2013).

[2] U. Abbondanno *et al.*, Measurements of fission cross sections for the isotopes relevant to the thorium fuel cycle (Meeting 24 September 2001), Boletín De La Sociedad Castellonense De Cultura **63**, 219 (2001).

[3] W. E. Parker *et al.*, Intermediate structure in the neutron-induced fission cross section of ^{236}U, Phys. Rev. C **49**, 672 (1994).

[4] J. W. Behrens and G. W. Carlson, Measurements of the neutron-induced fission cross sections of ^{234}U, ^{236}U, and ^{238}U relative to ^{235}U from 0.1 to 30 MeV, Nucl. Sci. Eng. **63**, 250 (1977).

[5] P. W. Lisowski *et al.*, Fission cross sections ratios for ^{233,234,236}U relative to ^{235}U from 0.5 to 400 MeV, in *Nuclear Data for Science and Technology*, Research Reports in Physics, edited by S. M. Qaim (Springer, Berlin, Heidelberg, 1992), pp. 732–733.

[6] R. Sarmento *et al.* (The n_TOF Collaboration), Measurement of the ^{236}U(n, f) cross section from 170 meV to 2 MeV at the CERN n_TOF facility, Phys. Rev. C **84**, 044618 (2011).

[7] R. O. Hughes *et al.*, Utilizing (p, d) and (p, t) reactions to obtain (n, f) cross sections in uranium nuclei via the surrogate-ratio method, Phys. Rev. C **85**, 024613 (2012).

[8] F. Tovesson, A. Laptev, and T. S. Hill, Fast neutron–induced fission cross sections of ^{233,234,236,238}U up to 200 MeV, Nucl. Sci. Eng. **178**, 57 (2014).

[9] A. Tsinganis, Measurement of the ^{236}U(n, f) cross-section at fast neutron energies with micromegas detectors, International Conference on Nuclear Data for Science and Technology Report I401, 2019, China (unpublished).

[10] H. T. Jing *et al.*, Studies of back-streaming white neutrons at CSNS, Nucl. Instrum. Methods Phys. Res. A **621**, 91 (2010).

[11] Q. An, H. Y. Bai, and J. Bao *et al.*, Back-n white neutron facility for nuclear data measurements at CSNS, J. Instrum. **12**, 07022 (2017).

[12] Y. Yang *et al.*, A multi-cell fission chamber for fission cross-section measurements at the Back-n white neutron beam of CSNS, Nucl. Instrum. Methods Phys. Res. A **940**, 486 (2019).

[13] J. Y. Tang *et al.*, Proposal for muon and white neutron sources at CSNS, Chin. Phys. C **34**, 121 (2010).

[14] J. Wen, Y. Yang, and Z. Wen *et al.*, Measurement of the U-238/U-235 fission cross section ratio at CSNS - Back-n WNS, Ann. Nucl. Energy **140**, 107301 (2020).

[15] R. Brun and F. Rademakers, ROOT — An object oriented data analysis framework, Nucl. Instrum. Methods Phys. Sect. Res. A **389**, 81 (1997).

[16] D. L. Shpak, G. G. Korolev, and K. D. Androsenko, Measurement of the fission cross section of ^{236}U relative to ^{235}U in the range of neutron energies between 0.50–3.72 MeV, Soviet At. Energ. **69**, 998 (1990).

[17] Y. Chen *et al.*, Neutron energy spectrum measurement of the Back-n white neutron source at CSNS, Euro. Phys. J. A **55**, 115 (2019).

[18] J. Zhang, A unified hauser-feshbach and exciton model for calculating double-differential cross sections of neutron-induced reactions below 20 MeV, Nucl. Sci. Eng. **114**, 55 (1993).

[19] Y. Han, Y. Xu, H. Liang, H. Guo, and Q. Shen, Global phenomenological optical model potential of nucleon-actinide reaction for energies up to 300 MeV, Phys. Rev. C **81**, 024616 (2010).

[20] Y. Han, Y. Shi, and Q. Shen, Deuteron global optical model potential for energies up to 200 MeV, Phys. Rev. C **74**, 044615 (2006).

[21] Y.-L. Xu, H.-R. Guo, Y. Han, and Q.-B. Shen, Applicability of the systematic helium-3 potential for triton-nucleus reactions, Int. J. Mod. Phys. E **24**, 1550005 (2015).

[22] X. Su and Y. Han, Global optical model potential for alpha projectile, Int. J. Mod. Phys. E **24**, 1550092 (2015).

[23] D. L. Hill and J. A. Wheeler, Nuclear constitution and the interpretation of fission phenomena, Phys. Rev. **89**, 1102 (1953).

[24] A. Gilbert and A. G. W. Cameron, A composite nuclear-level density formula with shell corrections, Can. J. Phys. **43**, 1446 (1965).

[25] Young, Chadwick, MacFarlane, IAEA, ENDF/B-VIII.0 database, LANL http://www-nds.iaea.org/exfor/endf.htm.

[26] O. Iwamoto, T. Nakagawa *et al.*, IAEA, JENDL-4.0 database, JAEA+ http://www-nds.iaea.org/exfor/endf.htm.

[27] G. Y. Tang, C. H. Cai, IAEA, CENDL-3.1 database, PKU, NKU http://www-nds.iaea.org/exfor/endf.htm.

Correction: A minor error in the cell to target distance given in the penultimate paragraph of Sec. IV B has been fixed.